

# LABORATORY OF RADIATION BIOLOGY

In 2010, the Laboratory of Radiation Biology (LRB) continued realization of the topic «Research on the Biological Action of Heavy Charged Particles with Different Energies» (04-9-1077-2009/2011) in the following fields: fundamental radiobiological and radiation genetics research with heavy charged particles; study-

ing the effect of accelerated charged particles on eye structures (the lens and retina); molecular dynamics research; mathematical modeling of induced mutagenesis in bacterial cells; and radiation research and radiation protection of JINR's basic facilities and the environment.

## RADIATION GENETICS AND RADIOBIOLOGY

New data were obtained on the regularities and mechanisms of the biological effect of accelerated charged particles in a wide range of linear energy transfer (LET) in the presence of replicative and reparative DNA synthesis inhibitors: cytosine arabinoside (Ara-C) and hydroxyurea (HU) [1]. The kinetics was studied of the induction and repair of DNA double-strand breaks (DSBs) in human peripheral blood lymphocytes under irradiation with particles in the LET range of 0.3–40 keV/ $\mu$ m.

It was shown that under charged particles, as well as under gamma radiation, effective DNA DSB repair

takes place in normal conditions. Under the modifying influence of Ara-C and HU, accumulation of DNA DSBs is observed after gamma irradiation, while after irradiation with accelerated heavy ions, the DNA DSB yield decreases (Fig.1). The obtained results show that under heavy charged particles in the presence of DNA synthesis inhibitors, DNA DSB repair takes place; but under gamma irradiation of cells, no DNA DSB repair is observed due to a large contribution by enzymatic DNA DSBs that are formed in the post-irradiation period in the course of the excision repair of nucleotides.

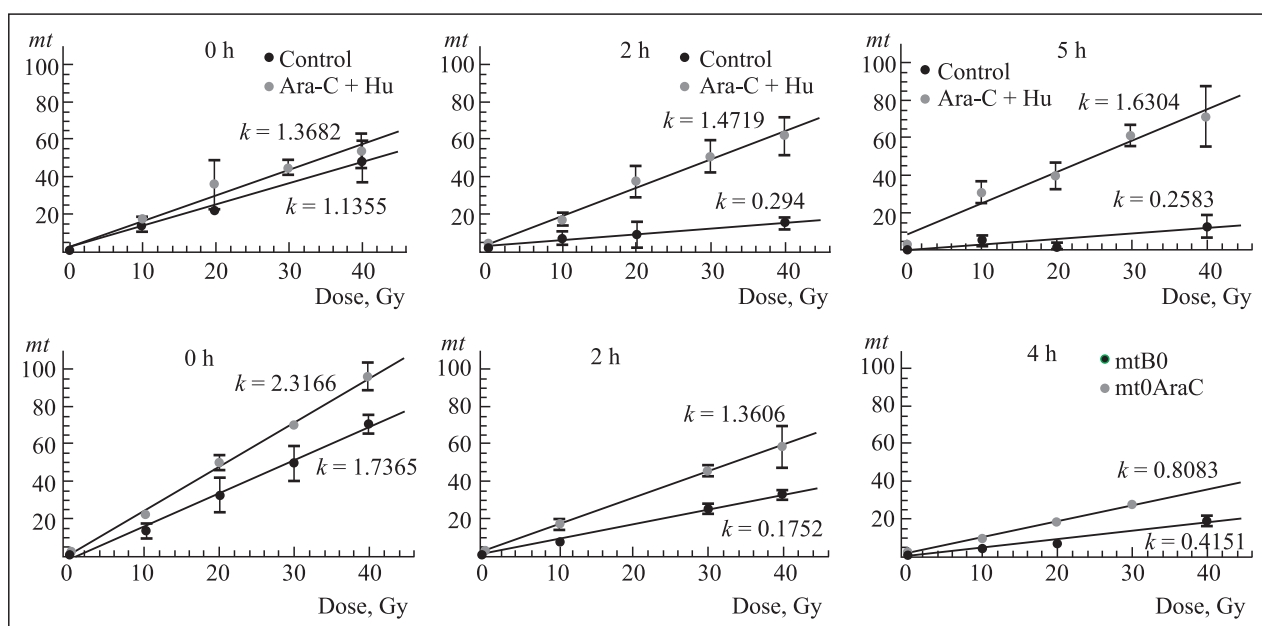


Fig. 1. The influence of DNA repair inhibitors (Ara-C and HU) on DNA DSB induction at different time after irradiation with gamma quanta and accelerated boron ions

HPRT mutant subclones of V79 Chinese hamster cells were studied which had been induced by different doses of gamma quanta and accelerated  $^{14}\text{N}$  and  $^7\text{Li}$  ions (with LET of  $\sim 77$  and  $\sim 20$  keV/ $\mu\text{m}$ , respectively) [2]. Mutants were identified with increased levels of chromosome aberrations as compared with intact control cells. The highest chromosome instability was observed among spontaneous mutant subclones and  $^7\text{Li}$  ion-induced ones. With increasing LET of radiations up to  $\sim 80$  keV/ $\mu\text{m}$ , the share of mutant subclones with an increased level of chromosome aberrations decreases (Fig. 2).

Experiments were continued to study the influence of reactive oxygen species (ROS) and a number of protein kinases on the formation of chromosome aberrations in cells under low doses of ionizing radiation. A nonlinear character of the survival rate and chromosome aberration yield dependence on the dose in the low dose region (up to 0.5 Gy) was shown earlier in different cell lines, including human normal and tumor cells. It was found that there is a hypersensitivity region in the initial part of the dose-effect curve, which is followed by a sharp increase in radioresistance with further increasing the dose. The mechanisms underlying this phenomenon have not yet been established.

The analysis of the cytoprotective properties of a number of proteins, the activation of which is regulated by the intracellular ROS level, allowed identification of

two most probable proteins providing higher radioresistance at lower doses: the ERK and p38 protein kinases. To study the role of these proteins in the low radiation dose effects, different modifiers were used: a free radical interceptor, a mitochondrial ROS generation inhibitor, and inhibitors of ERK and p38 activity. The yield of chromosome aberrations in human breast carcinoma cells (the cal51 line) was studied depending on the  $^{137}\text{Cs}$  gamma radiation dose.

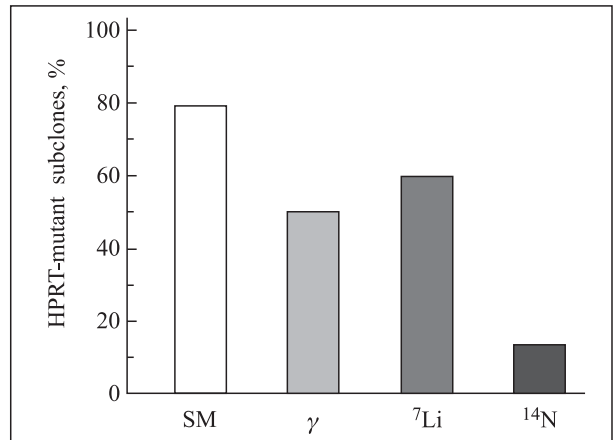


Fig. 2. The frequency of HPRT-mutant subclone formation with an increased level (compared to the control one) of chromosome aberrations induced by gamma quanta ( $\gamma$ ), lithium ions ( $^7\text{Li}$ ), and nitrogen ( $^{14}\text{N}$ ) ions. SM denotes spontaneous mutants

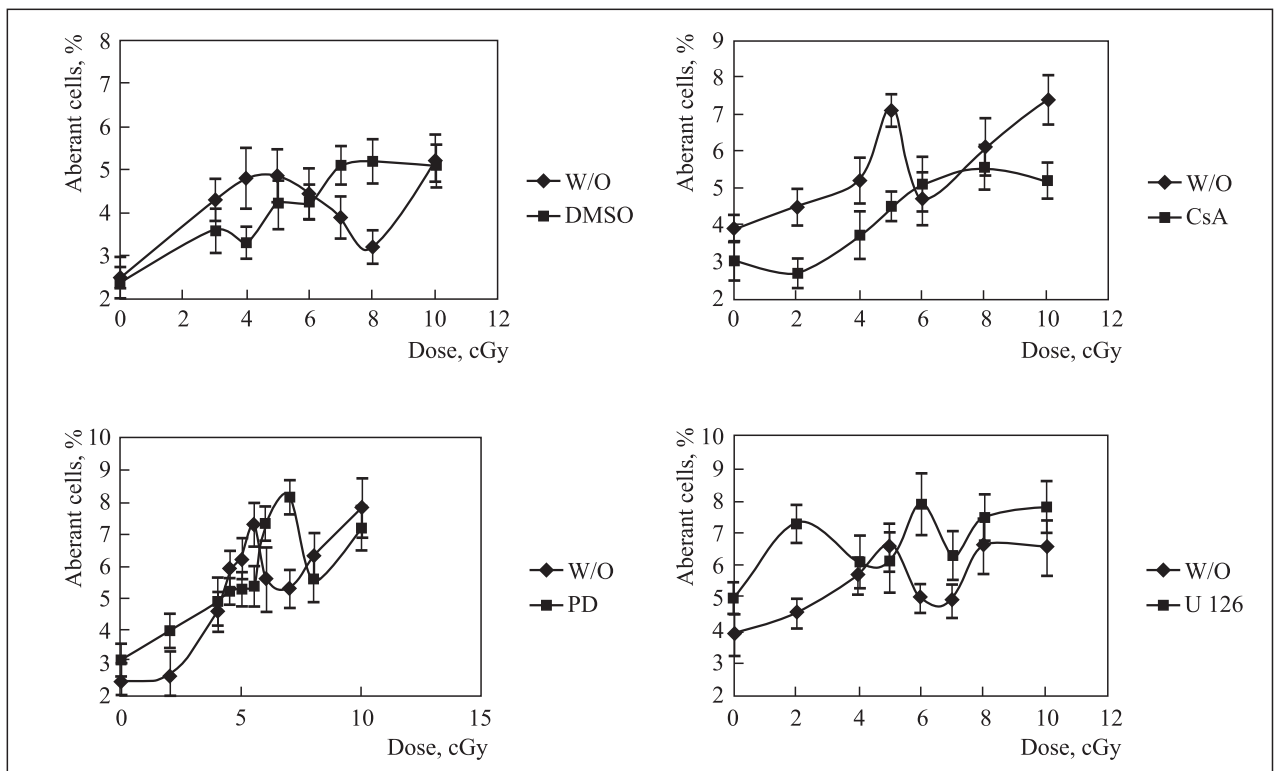


Fig. 3. Influence of different inhibitors (DMSO, cyclosporine A (CsA), PD98059, and U126) on the yield of aberrant cal51 cells under low doses of gamma radiation. W/O is the dose dependence of the yield of aberrant cells without a modifier

It was found that all used inhibitors modify the dose–effect curve shape (Fig. 3). The analysis of their influence on the yield of aberrant cells allowed concluding that hypersensitivity in the low-dose region is caused by the radiation-induced generation of intracellular ROS, the respiratory chain of mitochondria and NADPH oxidase being the source of these highly mutagenic radicals. An increase in radioresistance with further increasing the dose requires neither of the protein kinases used in this work (ERK and p38).

Taking into account available indications that apoptotic cell death can be initiated by the accumulation of single-strand DNA during repair, the frequency was studied of human blood lymphocyte apoptosis in the post-irradiation period in the presence of Ara-C and HU under irradiation with gamma quanta and accelerated Bragg peak protons (Fig. 4) [3].

It is established that in the presence of inhibitors, an increase is observed in the yield of apoptotic cells

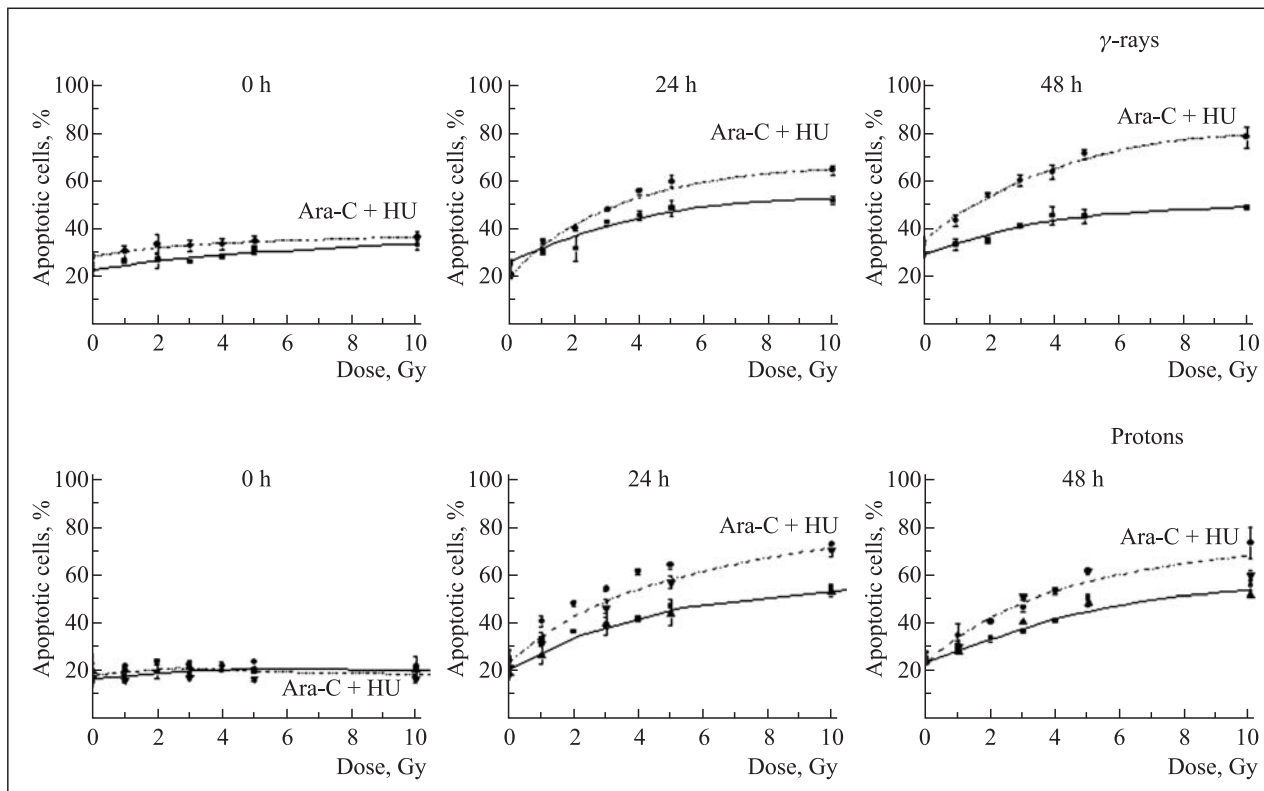


Fig. 4. Influence of DNA repair inhibitors (Ara-C and HU) on the induced apoptosis of human blood lymphocytes

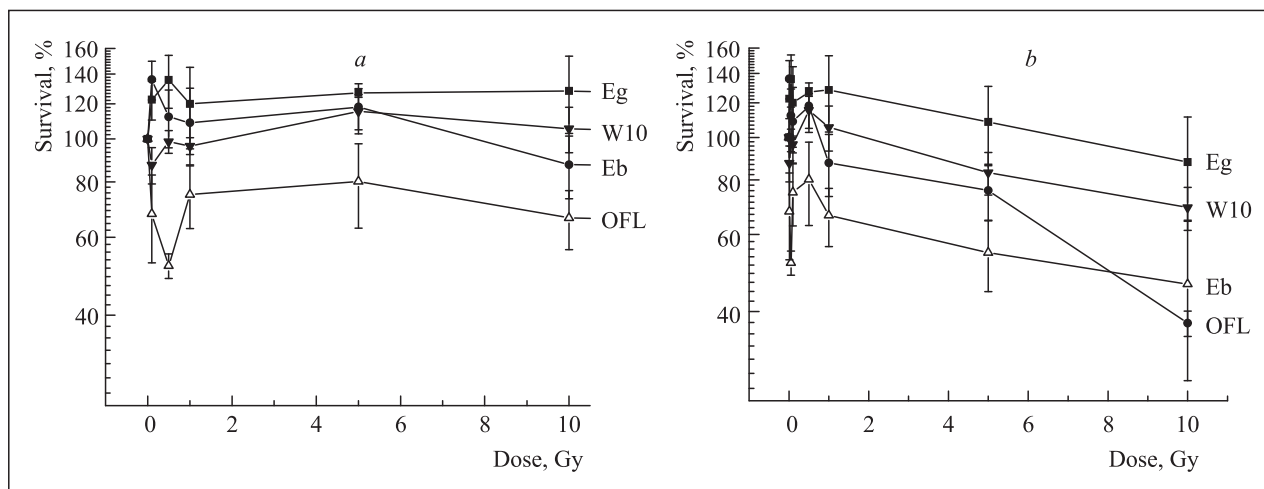


Fig. 5. The survival rate of *Euglena gracilis* cells of different genotypes after gamma irradiation: low doses (a); large doses (b). The survival rate was evaluated based on inoculation efficiency. The results are averaged over three experiments. The strains included *Euglena gracilis* (Eg), *Euglena bacillaris* (Eb), OFL, and W10

compared to cells under normal conditions. The maximal differences in the induced apoptosis levels are observed in 48 hours of post-irradiation cell incubation. With increasing LET of radiations, the modifying effect weakens, which correlates with data on DNA DSB induction by gamma quanta and accelerated heavy ions.

In 2010, research was continued on the mutagenic effect of heavy ions on saccharomycete yeast cells. Curves of the lethal and mutagenic effects of gamma radiation were defined more precisely. The influence of disorder in the functioning of mitochondria on the radiosensitivity and mutability of yeast cells was studied. Introduction was started of new methods of fluorescent

microscopy for identifying different types of eukaryote cell death, including necrosis and apoptosis induced by ultraviolet light and ionizing radiation. As a model system, unicellular eukaryotes were used: *Euglena* yeasts and algae.

In cooperation with Comenius University (Bratislava, Slovakia), the effect of low doses of radiation on *Euglena gracilis* with different genotypes was studied [4].

It was shown that irradiation of unicellular *Euglena* algae with gamma quanta at low doses (up to 10 Gy) has a stimulating effect (Fig. 5, a), and it is only above 100 Gy that irradiation causes cell death (Fig. 5, b).

## PHOTORADIOBIOLOGICAL RESEARCH

**Mechanisms of Mouse Retina Damage after Gamma and Proton Irradiation.** Irradiation of the retina with 170 MeV protons and gamma quanta at 14 Gy induced DNA damage (single- and double-strand breaks) combined with an increase in the level of the expression of P53- and ATM proteins. The expression of these proteins at such radiation dose went along with DNA repair, but not with retina cell death (Fig. 6).

Increasing the proton dose up to 25 Gy resulted in the death of photoreceptors, which was growing with time up to their full disappearance in 8–10 days (Figs. 7–9).

The death of photoreceptors was preceded by an increase in the expression of the FasR receptor and effector caspase-3 (24 hours) (Fig. 10) [5]. It points to the possibility of apoptosis initiation in the retina

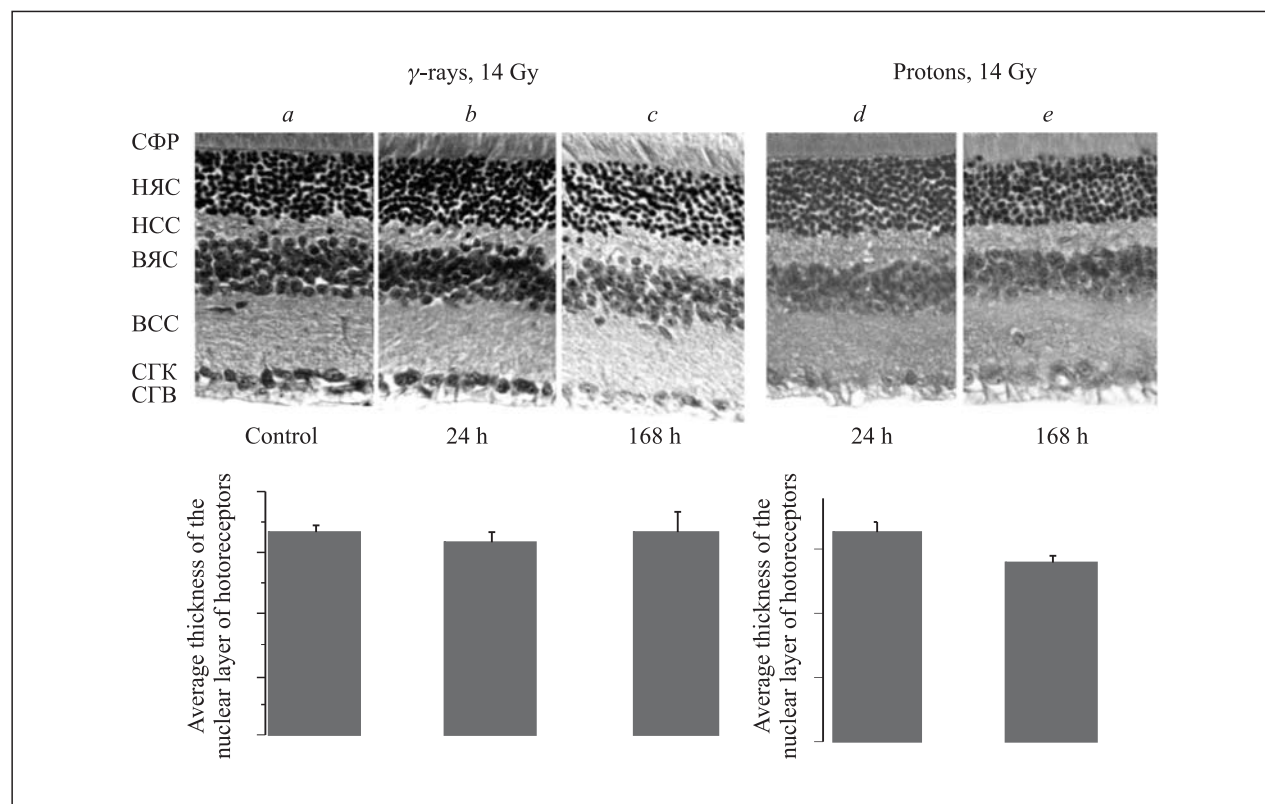


Fig. 6. Microphotographs of retina cuts of control mice and mice irradiated at 14 Gy with gamma rays and protons: control (a); 24 and 168 hours after gamma irradiation (b, c); 24 and 168 hours after proton irradiation (d, e)

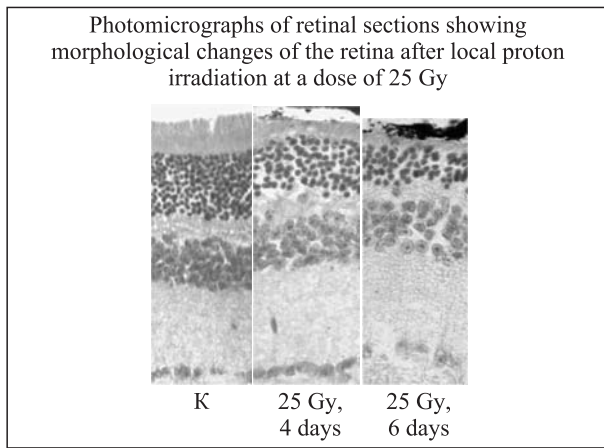


Fig. 7. Microphotographs of intact mouse retina cuts (K) and retina locally irradiated with protons at 25 Gy

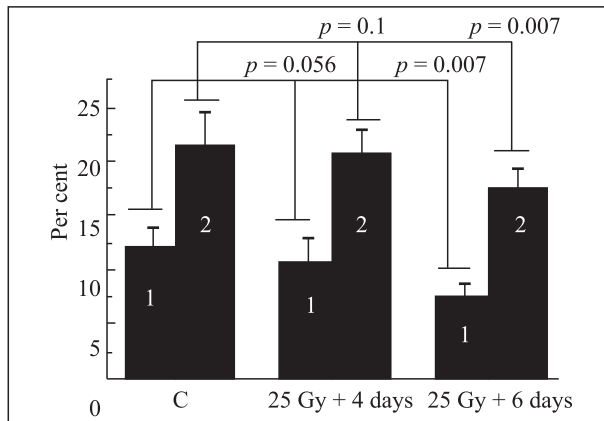


Fig. 8. The thickness of the layer of photoreceptor segments (1) and nuclear layer of photoreceptors (2) in the intact mouse retina (C) and 4 and 6 days after irradiation of mice with protons at 25 Gy. The layer thickness is shown in per cent of the total thickness of the retina.  $p$  is the significance level of the difference from the intact retina

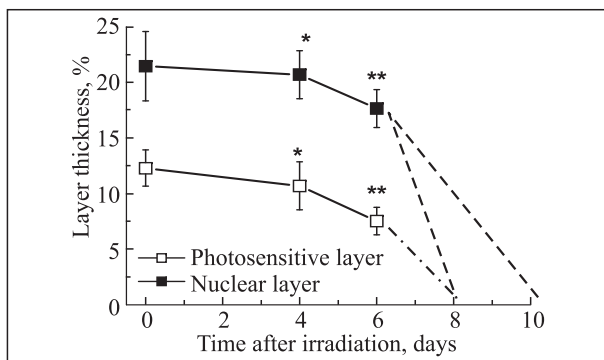


Fig. 9. The dynamics of the degeneration of the photosensitive and nuclear layers of the mouse retina in response to the irradiation of mice with protons at 25 Gy. The ordinate axis is the layer thickness in per cent of the total thickness of the intact retina. The average value  $\pm$  standard deviation is shown. The dotted line shows the extrapolation range of the expected changes. The significance level of the difference from the control ( $t = 0$ ):  $p > 0.05$ (\*);  $p < 0.01$ (\*\*)

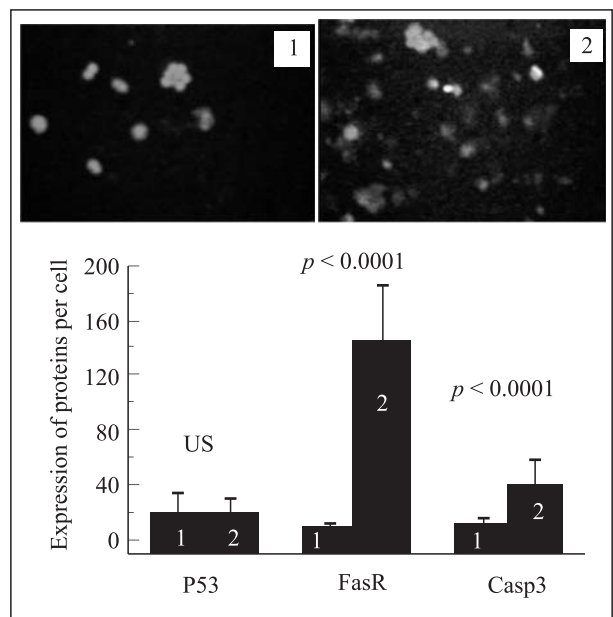


Fig. 10. Expression of proapoptotic proteins in response to proton irradiation: 1 — intact retina; 2 — proton irradiation 25 Gy

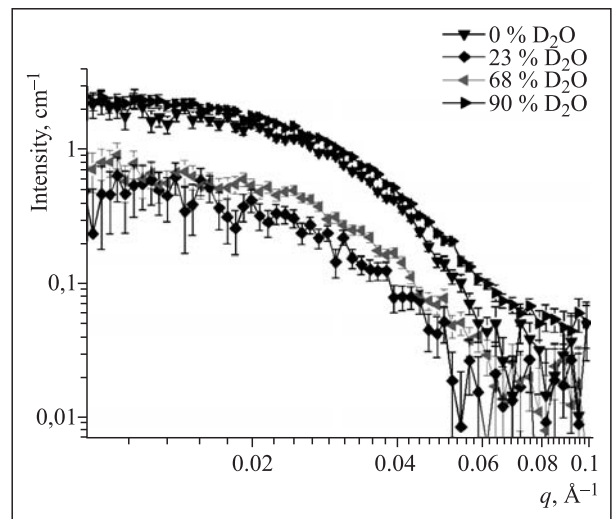


Fig. 11. Scattering curves for  $\alpha$ -crystalline solutions with different heavy-water content

after exposure to very high doses of radiation. In other words, the obtained data are the evidence of the high radioresistance of differentiated cells of the retina.

The results of this research are important for the evaluation of the risk of damaging the retina in long-term space flights, in industries involving radiation danger, at radiation emergencies, in radiotherapy (especially, in proton therapy), and in medical diagnostics.

**Studying the Spatial Structure of  $\alpha$ -Crystalline Oligomers with Small-Angle Neutron Scattering.** The structure of the  $\alpha$ -crystalline protein isolated from a bovine lens was studied by small-angle neutron scattering with contrast variation. The measurements were

conducted at the YuMO small-angle neutron spectrometer of the IBR-2 reactor, JINR (Fig. 11).

Based on the values of the inertia radius and functions of distribution by distance for different  $D_2O/H_2O$  ratios, new information was obtained about the protein mass, shape, and dimensions, and about heterogeneities within the macromolecule (as the heavy-water content in the medium was varied). It was concluded that the

scattering density in the  $\alpha$ -crystalline areas inaccessible to water is distributed homogeneously, and that  $\alpha$ -crystalline is deuterated uniformly throughout the whole oligomer value [6].

The conclusion on the  $\alpha$ -crystalline structure is important for the development of the  $\alpha$ -crystalline quaternary structure models, which are still absent.

## MATHEMATICAL MODELING OF RADIATION-INDUCED EFFECTS

A model was developed which describes key processes taking place in *Escherichia coli* (*E. coli*) bacterial cells during base excision repair (BER) [7, 8]. It is the first time that on the basis of the numerical modeling of a network of biochemical reactions, the mechanism is quantitatively described of the removal of damaged bases of the 8-oxoguanine (8-oxoG) type with the participation of formamidopyrimidine DNA glycosylase (the Fpg protein), which has several types of activity. The modeling results agree with *in vitro* experimental data characterizing the initial stages of the

repair process involving the Fpg protein (Fig. 12). The developed model allowed a quantitative assessment of changes in the concentration of the main BER enzymes and — for the first time — to predict the kinetics of the intermediate DNA states during damage repair. A quantitative assessment was made of the share of lesions that had not been removed at the repair stages determined by the Fpg protein activity. It was shown that this magnitude can be regarded as the characteristic of the failure probability during BER mechanism realization.

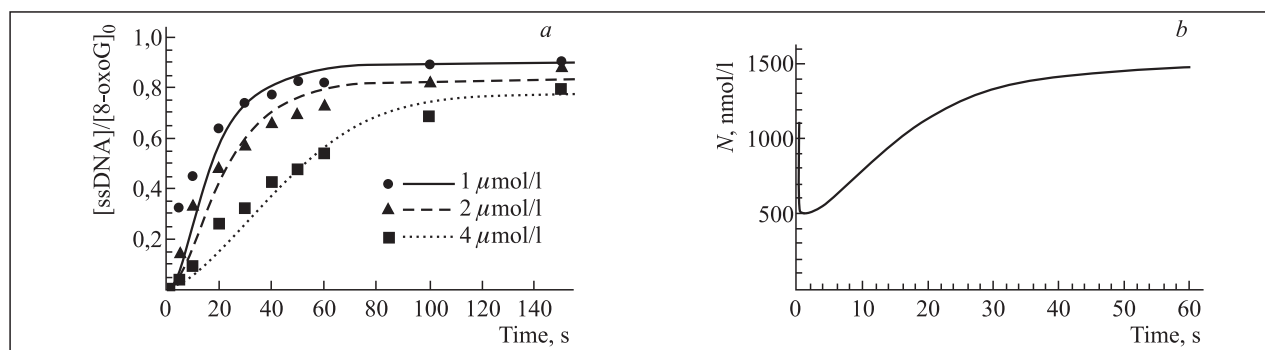


Fig. 12. The kinetics of 8-oxoguanine (8-oxoG) removal with the participation of the Fpg protein in comparison with experimental data (Fedorova O. S. et al., 2002) obtained at three different initial 8-oxoG concentrations: 1, 2, and 4  $\mu\text{mol/l}$  (a); the Fpg protein kinetics during BER (b)

A model was studied of the response of the genetic regulation system of *E. coli* bacterial cells to ultraviolet (UV) irradiation on the basis of the stochastic approach using the Gillespie algorithm. Compared to the earlier model of SOS response [9–11], it became possible to simulate intracellular biochemical processes in more detail. It is shown that at the level of a separate cell, the initial signal's time dependence consists of at least one maximum depending on the UV energy fluence. The model is applicable not only to the wild-type *E. coli*

bacterial cells, but also to UVR-mutant cells.

A quantitative assessment was made of UV-induced SOS response in *E. coli* bacterial cells with the disordered translesion synthesis function [12]. The dynamics was modeled of the concentration of the key proteins of the bacterial SOS system for *recA*, *umuD*, and *umuC* mutants of *E. coli*. The quantitative assessment was based on the earlier mathematical model of the induced mutation process in bacterial cells under UV radiation [9–11].

## COMPUTER MOLECULAR MODELING OF BIOPHYSICAL SYSTEMS

Correlations between the structural behavior of a number of wild-type and mutant proteins were studied. A molecular dynamics (MD) analysis was conducted

of the phase changes of a biphenyl molecule in an active medium: an  $HNO_3$  solution. Temperature and energy characteristics and phase changes of a biphenyl

molecule were studied; nontrivial phase changes of a biphenyl molecule exposed to different modes of interaction with the active solution were found and identified [13]. The effects of the self-organization of a liquid around a carbon nanotube were discovered and described. These effects are very important for understanding and describing the intracellular biological processes with a view to designing drugs and delivering them to a living cell [14]. Molecular mechanisms of ion transportation were studied on the basis of a MD research on the processes of the interaction between valinomycin and  $K^+$  and  $Na^+$  ions in water [15].

A series of studies were conducted on the structural and conformational properties of native and mutant rhodopsin. A computer modeling research was done on the molecular dynamics of the chromophore group (11-*cis*-retinal) of rhodopsin. Molecular dynamics was tracked in a span of 3 ns;  $3 \cdot 10^6$  discrete conformational states of the molecule were analyzed. It was shown that in approximately 0.3–0.4 ns after the modeling start, the  $\beta$ -ionone ring turns 50–60° around the C6–C7 bond relative to the initial configuration of 11-*cis*-retinal (Figs. 13, 14).

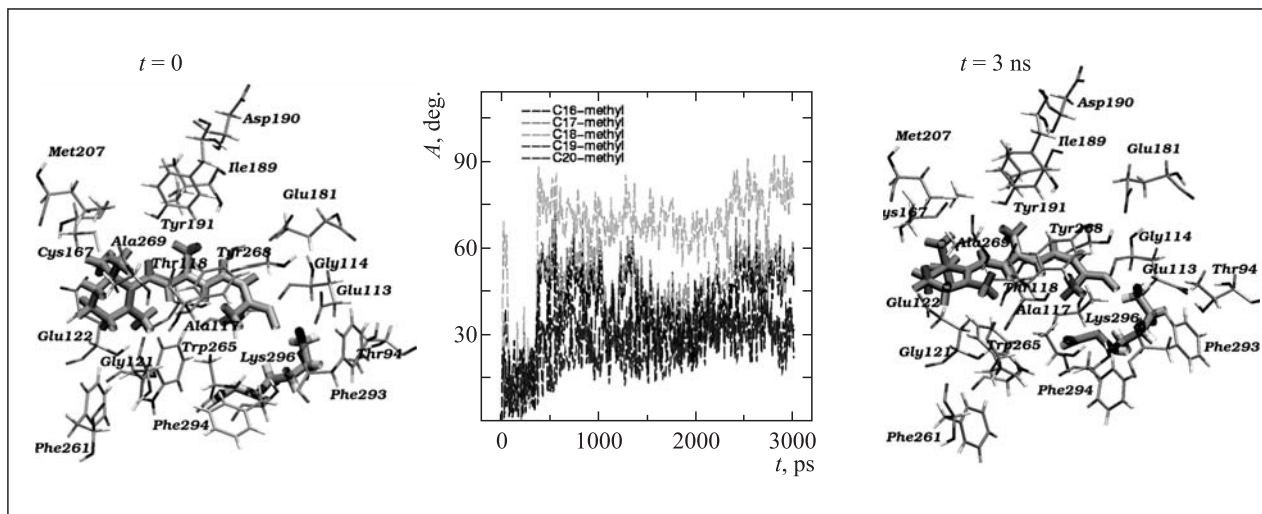


Fig. 13. The  $\beta$ -ionone ring of 11-*cis*-retinal is turned 50–60° off the polyene chain plane. The  $\beta$ -ionone ring of free 11-*cis*-retinal is planar with the polyene plane

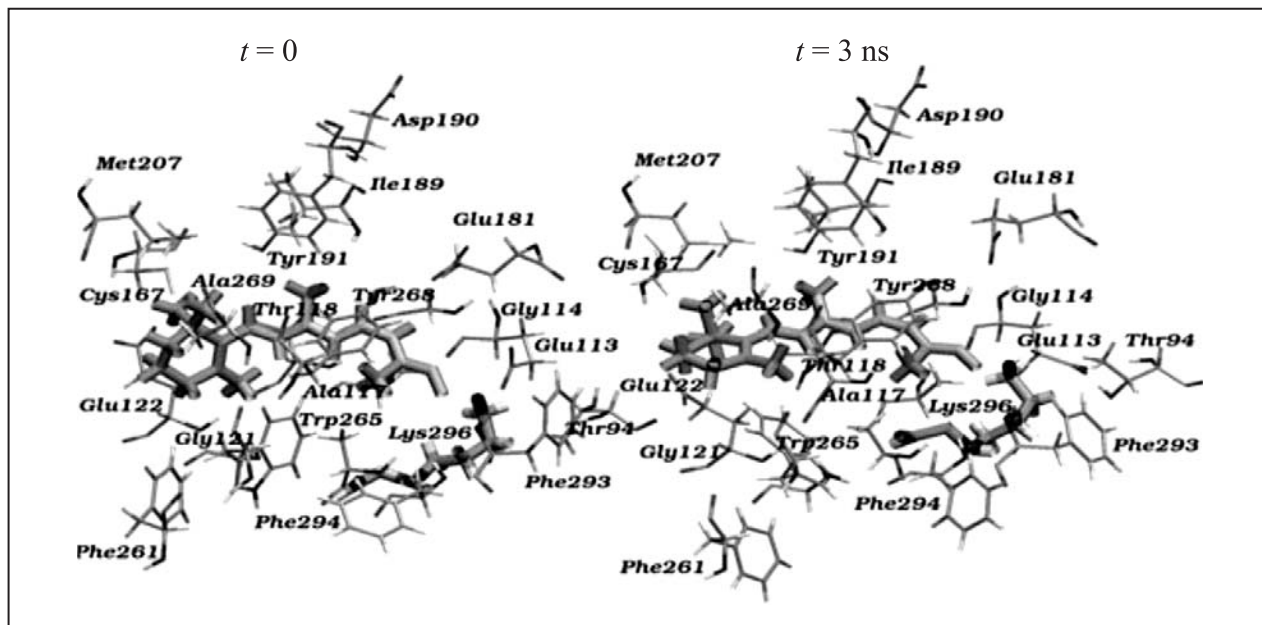


Fig. 14. Calculation results: the energy of the S0–S1 transition for the  $t = 0$  system is 2.95 eV; and for the  $t = 3$  ns system, 3.91 eV, which corresponds to a 10 nm shift of the absorption spectrum of the  $t = 3$  ns system towards longer waves. The calculation was done by the configuration interaction method taking into account single excitations and using the two-exponent valence basis with the addition of polarization functions (cc-pVDZ). PC GAMESS software was used (a qualitative estimation was made)

With the use of nonempirical methods of quantum chemistry, the locations were estimated of the maxima of the rhodopsin absorption lines in different conformational states ( $t = 0$  and 3 ns). It was found that the maximum of the absorption line of the molecule in the final state of the modeling time span ( $t = 3$  ns) is shifted 10 nm towards longer waves from the initial state ( $t = 0$ ). It means that the energy of the transition of such system into the excited S1 singlet state after

light quantum absorption is lower than the one when the  $\beta$ -ionone ring of chromophore is planar with the plain of its polyene chain.

It is assumed that this change in the spatial configuration of 11-*cis*-retinal can play a very important role in the ultrafast (shorter than 200 fs) and efficient (with a quantum yield of 0.65) photochemical reaction of chromophore isomerization in the chromophore center of the rhodopsin molecule.

## RADIATION PROTECTION PHYSICS AND RADIATION RESEARCH

The development was continued of the radiation-safety measures for the NICA accelerator complex, which is being designed at JINR. Using GEANT4 software, the collider shielding was calculated as regards the accumulation of Au nuclei with an energy of 4.5 GeV/u taking into account the losses of nuclei distributed uniformly over the rings and local losses at the beam interceptors [16]. A shielding configuration was proposed that would provide compliance with the annual-dose limit for general population at the border of the buffer area from multiply scattered neutrons and gamma quanta. For the State Specialized Planning Institute (GSPI Corporation), initial data were prepared for shielding engineering calculations (double differential cross sections of  $^{197}\text{Au} + ^{\text{nat}}\text{Fe}$  interaction at the energy of nuclei of 4.5 GeV/u, coefficients of neutron fluence attenuation in concrete, and air activation within the collider shielding).

Cooperation was continued between JINR and the Institute of Space Research, the Russian Academy of

Sciences, on the programme of planet research with nuclear physics methods. In particular, work was continued on studying the characteristics of neutron detectors and gamma spectrometers and their gauging for the following missions: LRO (LEND), Phobos Ground (HEND Phobos), MSL (DAN), ISS (BTN-Neutron), and BEPI Colombo (MGNS) [17]. A  $\text{LaBr}_3$  detector was gauged for the energies of gamma quanta up to 10 MeV — at isotope sources and with gamma quanta of radiation neutron capture reactions and inelastic neutron scattering. Using track detectors, the fragmentation of 370 MeV/u  $^{20}\text{Ne}$  and 470 MeV/u  $^{24}\text{Mg}$  nuclei was studied in light targets [18]. Development was continued of a portable stand-alone neutron spectrometer in a wide energy spectrum based on the multisphere technique. A composite polyethylene moderator was developed and produced which allows significant reduction in the total weight and overall dimensions of the device.

## REFERENCES

1. Boreyko A. V. *et al.* Influence of DNA Synthesis Inhibitors on the Induction and Repair of DNA Double-Strand Breaks in Human Blood Lymphocytes under Radiations with Different LET // Part. Nucl., Lett. 2011. V. 8, No. 4(167). (in Russian) (in press).
2. Koshlan I. V., Koshlan N. A., Govorun R. D. Chromosome Instability of HPRT-Mutant Subclones Induced by  $^{14}\text{N}$  and  $^7\text{Li}$  Ions and Gamma Quanta // Proc. of the IV Sissakian Readings «Problems of Biochemistry and Radiation and Space Biology», Dubna, 2010 (in Russian) (in press).
3. Baranova E. V. *et al.* The Influence of Modifying Factors on Radiation Induced Apoptosis in Human Lymphocytes. Rapid Diagnosis in Population at Risk from Radiation and Chemicals // Proc. of the NATO Advanced Training Course on Rapid Diagnosis in Population at Emergency and Risk / Eds.: A. Cebulka *et al.* IOS Press, 2010. P. 261–266.
4. Zhuchkina N. I. *et al.* Research on the Effect of Gamma Radiation on Euglena Gracilis Algae // Proc. of IV Sissakian Readings «Problems of Biochemistry and Radiation and Space Biology», Dubna, 2010 (in Russian) (in press).
5. Tronov V. A. *et al.* Photoreceptor Death and Retina Degeneration in Mice in Response to Genotoxic Influence (Ionizing Radiation and the Methylating Agent) // Cytology. 2011. V. 53 (in Russian) (in press).
6. Krivandin T. N. *et al.* Research on the  $\alpha$ -Crystalline Structure Using Small-Angle Neutron Scattering with Contrast Variation // Biochemistry. 2010. V. 75, No. 11. P. 1499–1507 (in Russian).
7. Belov O. V. Stochastic Simulation of Base Excision Repair in Escherichia Coli Bacterial Cells // Molecular Simulation Studies in Material and Biological Sciences: Book of Abstracts of the 4th Japan–Russia Intern. Workshop «MSSMBS'10», Dubna, Sept. 26–29, 2010. P. 36–37.
8. Belov O. V. Modeling Excision Repair of Damaged Bases in Escherichia Coli Bacterial Cells // Part. Nucl. Lett. 2011. V. 8, No. 2(165). P. 241–251 (in Russian) (in press).
9. Belov O. V., Krasavin E. A., Parkhomenko A. Yu. Math-

- emational Model of Induced Mutagenesis in Bacteria *Escherichia Coli* under Ultraviolet Irradiation // Biophysics. 2010. V. 55, No. 4. P. 682–690.
10. Belov O. V., Krasavin E. A., Parkhomenko A. Yu. Modelling of the Induced Mutation Process in Bacterial Cells // Proc. of the NATO Advanced Training Course on Rapid Diagnosis in Population at Emergency and Risk, Krakow-Zakopane, Poland. Oct. 19–24, 2009 / Eds.: Cebulska-Wasilewska A. and Osipov A. Sub-Series E: Human and Societal Dynamics. IOS Press BV, 2010. V. 73. P. 307–312.
  11. Belov O. V., Krasavin E. A., Parkhomenko A. Yu. Mathematical Modeling of the Induced Mutation Process in Bacterial Cells // AIP Conf. Proc. 2010. V. 1204. P. 249–250.
  12. Belov O. V. Modeling Ultraviolet-Induced SOS-Response in Translesion Synthesis-Deficient Cells of *Escherichia Coli* Bacteria // Part. Nucl., Lett. 2011. V. 8, No. 1(164). P. 61–66.
  13. Kholmurodov Kh. T., Chulkova A. S., Yasuoka K. Molecular Dynamics Study of the Effect of Electrostatic Interactions on the Biphenyl Structure in the Active HNO<sub>3</sub> Solvent // The Open Physical Chemistry J. 2010. V. 4. P. 10–16.
  14. Kholmurodov Kh. T., Abasheva M. S., Yasuoka K. Molecular Dynamics Simulations of Valinomycin Interactions with Potassium and Sodium Ions in Water Solvent // Advances in Biosci. and Biotechnol. 2010. V. 1, No. 3. P. 145–240.
  15. Kholmurodov Kh. T., Aru G. F., Yasuoka K. Molecular Dynamics Simulations of the Interaction of Carbon Nanotube and a Carbon Disulfide Solvent // Nat. Sci. 2010. V. 2, No. 8. P. 902–910.
  16. Техническое задание на разработку проектной документации размещения ионного коллайдера NICA в здании 205 ЛФВЭ ОИЯИ в г. Дубне. 318Б-059-Т31. Дубна, 2010.
  17. Beskrovnaia L. et al. Simulation of Residual Activity in Steel and Copper Targets Induced by 950 MeV/nucl. Uranium Ions // Part. Nucl., Lett. 2011. V. 8, No. 4(167) (in press).
  18. Golovchenko A. et al. Fragmentation of 370 MeV/nucl. <sup>20</sup>Ne and 470 MeV/nucl. <sup>24</sup>Mg in Light Targets // Rad. Meas. 2010. V. 45, No. 7. P. 856–860.